Real-time VR Simulation of Laparoscopic Cholecystectomy based on Parallel Position-based Dynamics in GPU

Junjun Pan [†*]
State Key Lab of VR Tech & Syst
Beihang University
Peng Cheng Lab

Leiyu Zhang [†]
State Key Lab of VR Tech & Syst
Beihang University

Peng Yu [†]
State Key Lab of VR Tech & Syst
Beihang University

Yang Shen
Faculty of Education
Beijing Normal University

Haipeng Wang
Beijing Aerospace General Hospital

Haimin Hao
Beihang University
Peng Cheng Lab

Hong Qin [*]
Department of Computer Science
Stony Brook University

ABSTRACT

In recent years, virtual reality (VR) based training has greatly changed surgeons learning mode. It can simulate the surgery from the visual, auditory, and tactile aspects. VR medical simulator can greatly reduce the risk of the real patient and the cost of hospitals. Laparoscopic cholecystectomy is one of the typical representatives in minimal invasive surgery (MIS). Due to the large incidence of cholecystectomy, the application of its VR-based simulation is vital and necessary for the residents' surgical training. In this paper, we present a VR simulation framework based on position-based dynamics (PBD) for cholecystectomy. To further accelerate the deformation of organs, PBD constraints are solved in parallel by a graph coloring algorithm. We introduce a bio-thermal conduction model to improve the realism of the fat tissue electrocautery. Finally, we design a hybrid multi-model connection method to handle the interaction and simulation of the liver-gallbladder separation. This simulation system has been applied to laparoscopic cholecystectomy training in several hospitals. From the experimental results, users can operate in real-time with high stability and fidelity. The simulator is also evaluated by a number of digestive surgeons through preliminary studies. They believed that the system can offer great help to the improvement of surgical skills.

Index Terms: Human-centered computing—Human computer interaction—Interactive systems and tools—User interface programming; Computer systems organization—Real-time systems—Real-time system architecture

1 INTRODUCTION AND MOTIVATION

As one of the modern minimally invasive procedures, laparoscopic surgery has become popular primarily because of its small wounds and rapid recovery. For instance, nearly 15 million laparoscopic procedures are performed globally annually [21]. Laparoscopic cholecystectomy (LC) is one of the typical representatives. However, in reality the number of laparoscopic surgeons cannot meet the huge demand in clinic. One reason is that the learning curve of laparoscopic surgery is very long. In the narrow operation space, mistakes may easily occur if surgeons do not handle procedures properly. It usually takes about ten years to became a laparoscopic surgeon for resident. Traditional training approaches of laparoscopic surgeries are usually on animals or corpses, which could give rise to negative effects, such as high cost, low practice opportunities, and related ethical issues. These problems have become bottleneck for the development of laparoscopic surgery skill training. The advent of VR surgical simulator has changed this situation. It not only reconstructs the real surgical environment and procedures, but also can be reused for a variety of designed training tasks. Therefore, many institutions and commercial companies, such as Lap Mentor [24], LapVR CAE Healthcare Interventional Simulator [8], and the LapSim Surgical Science Simulator [23] have carried out research and development on VR medical simulators. Whereas, to our knowledge, there is no paper that elaborates the whole laparoscopic cholecystectomy procedure and the development details. This paper presents a framework of virtual laparoscopic cholecystectomy. For the deformation of soft tissue, we propose the algorithm to parallelize position-based dynamics (PBD) through graph coloring. To simulate electrocautery, we introduce the bio-thermal conduction model to modify the topology of gallbladder fat tissue. For the separation of liver and gallbladder, a hybrid multi-model connectivity method is designed to handle the interactions and visual rendering. Compared with the work of Kim et al. [11], the experimental results confirms that our technique is more efficient in soft tissue deformation. Finally, a questionnaire is designed to evaluate the utility experience of our system by digestive surgeons.

The simulator (Fig. 1) hardware consists of a touch screen, two surgical instrument handles, a foot pedal, a Bluetooth mouse, and a computer with two haptic devices. We choose Geomagic Touch (Phantom Omni, Sensible) as the haptic feedback device of our simulator. It could offer 6 degree-of-freedom (DOF) input data with a resolution of 0.009 mm in 3D space, and up to 3.3 N 3 DOF force output [25]. The software is developed with OpenHaptics, GLSL, CUDA, and C++. The anatomy models are obtained from the human anatomy database [9], which contains the gallbladder, liver, abdominal wall, bile duct, and cystic duct/artery.

Fig. 2 illustrates the software architecture of our system, which includes two phases: offline and online. The offline phase consists of loading the geometric model, initializing the physical model (creating stretching constraints and volume constraints), and coloring the physical model using the graph algorithm. For the online phase, the system first detects collision based on the data sent by the force feedback device, then calculates the potential distribution of the model and solves the constraints in parallel for the soft tissue deformation, and finally updates the model texture and shape in a graphic and tactile manner. In technical essence, there are three innovative contributions:

- We propose a deformation model of soft tissue based on graph coloring parallel acceleration, within the position-based dynamics (PBD) framework.
- The laws of thermodynamics is employed in the electrocautery simulation. A bio-thermal conduction model is presented to improve the realism of fat tissue burning.

[*]Corresponding authors: pan_junjun@buaa.edu.cn, qin@cs.stonybrook.edu.
[†]These authors contributed equally to this work.

2642-5254/20/$31.00 ©2020 IEEE
DOI 10.1109/VR46266.2020.00076

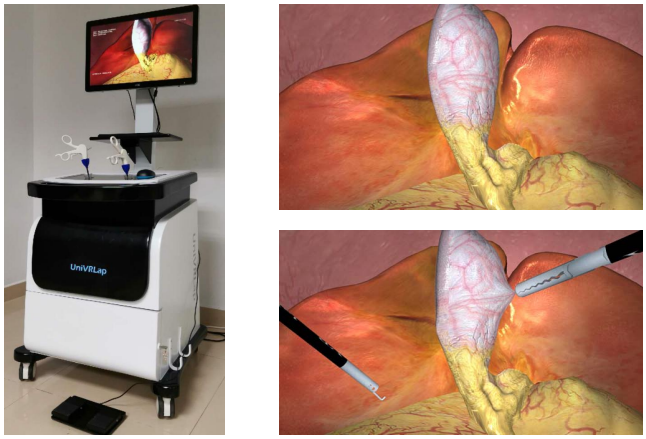

(a) (b)

Figure 1: Overview of our developed VR laparoscopic surgery simulator. (a) Hardware interface; (b) Software interface of laparoscopic cholecystectomy training.

- We design a hybrid multi-model connection method, which can simulate the separation of the gallbladder from liver in real-time.

2 Related Works

The first surgical simulator was born at the end of the 19th century, Delp et al. [3] established a simulation system for observing the ankle and joint surgery process and results. With further development of hardware devices, the virtual surgery simulation system has been improved. The surgical simulator developed by Boston Dynamics with force feedback uses the Phantom series of force feedback devices [29], which greatly enhances its realism and practicality. Many scholars have also conducted a large amount of research work on the soft tissue deformation and electrocautery simulation based on biomechanical properties.

Physics-based modeling methods are widely used in simulations at present. The mass spring system (MSS) has been used in facial modeling, and human body simulation [5, 17]. But it hardly characterizes the volume of the model when deformation occurs, and it is quite tedious to tune the stiffness parameters of the model. Another popular method is the finite element method (FEM) with high precision and good flexibility. It has been applied in liver and ophthalmic surgery simulation [15, 26, 28]. However, for more complex surgical scenarios, its poor computational performance (e.g., not real-time) becomes a disadvantage that cannot be ignored. Position-based dynamics (PBD) [18] is a widely utilized approach in interactive environments because it is fast, stable, and controllable. To solve the system dynamic equation, PBD employs a non-linear Gauss-Seidel solver which is not suitable for parallel computation. Although Jacobian methods are easy to be implemented on GPU, they might suffer from stability problems.

To accelerate the simulation of soft tissue deformation in virtual surgery, one effective solution is the graph coloring algorithm, which is a classic problem in computer science. For an undirected graph $G = (V, E)$, V represents the set of all the vertices in the graph, E represents the set of all the edges in the graph. The graph coloring problem refers to dividing all the vertices into a number of sets. The vertices in each set are dyed in the same color, and any two vertices with the same color do not share an edge. The optimal graph staining results have the smallest number of colors and a uniform number of vertices in each color. In parallel computing, some interrelated data structures are not capable of parallel computing. The graph coloring algorithm provides a solution, which abstracts the target problem into a graph and each sub-question is treated as a vertex, then the vertices dyed with the same color can be safely parallelized. Therefore, the graph coloring algorithm has wide applications in scientific computation and numerical optimization. Luby et al. [14] proposed a dyeing algorithm based on the largest independent set. The basic idea is to find the most likely large independent set of colors iteratively until all the vertices are dyed. Jones et al. [10] improved Luby's algorithm to reduce the number of colors and iterations by changing the way the adjacent vertices are colored. Grable et al. [7] proposed a random dyeing disc coloring algorithm. The color number of each vertex is initialized to a coloring disc, and then the vertices are randomly colored until all vertices are colored. Fratarcangeli et al. [6] applied this method to the field of dynamic physics simulation and achieved a significant acceleration effect of projection dynamics. Tas et al. [27] designed a greedy heuristic coloring algorithm, which is more optimistic.

Electrocautery is also a common operation in surgery, in which L-hook burns soft tissues by high-frequency current. Many scholars have presented their research work about the biological characteristics of human tissue [22]. Dodde et al. [4] analyzed the electrothermal transformation and heat distribution of tissue based on finite element model of electro-thermal coupling. Lu et al. [13] extended it to the soft tissue burning system based on FEM and proposed a method for topological change of the tetrahedral model. Kim et al. proposed a grid engraving algorithm [12], which employs the volume field to capture the modification of the model surface by L-hook. They combined the engraving algorithm with FEM to simulate the soft tissue electrocautery process. Then they applied this method to the laparoscopic cholecystectomy simulator [11]. Berndt et al. [2] utilized empirical parameters to define the thermal response thresholds which are employed to simulate different organs and tissues, including muscle, fat, and bone.

3 Proposed Method

3.1 PBD Model based on Graph Coloring Algorithm

3.1.1 Deformation of Soft Tissue

In VR simulation of laparoscopic cholecystectomy, soft tissue deformation is one of rather fundamental and important technical problems. It is quite challenging to deform the geometry of a fine organ accurately in real-time with limited computational resources. Compared to low-precision MSS and high-cost FEM, the position-based dynamics (PBD) provides an alternative solution for soft tissue deformation that meets certain physical laws [16, 18]. It eliminates the calculation process of acceleration [19], and directly updates the velocity and position of vertices after the external force is generated, then corrects the predicted position through a series of constraints. Therefore, PBD greatly speeds up the solution of equations and improve the real-time performance. Meanwhile, some scholars proved that extended PBD can be applied to the real-time dissection simulation of soft tissue with topology changes [20]. Here we choose PBD as the deformation model in our simulation system.

At the offline stage, the first step is to create constraints for the gallbladder, liver, fat, and tubular tissue within the framework of the PBD. We initialize n vertices $\mathbf{P} = (\mathbf{p}_1, \ldots, \mathbf{p}_n)$ of the model with the velocities $\mathbf{v} = (\mathbf{v}_1, \ldots, \mathbf{v}_n)$, positions $\mathbf{x} = (\mathbf{x}_1, \ldots, \mathbf{x}_n)$, masses $m = m_1, \ldots, m_n$, and colors $\mathbf{col} = (\mathbf{c}_1, \ldots, \mathbf{c}_n)$. The constraints we impose on soft objects are as follows:

Distance constraints: It can be represented by:

$$C_{distance}(\mathbf{p}_1, \mathbf{p}_2) = \|\mathbf{p}_1 - \mathbf{p}_2\| - d, \tag{1}$$

where $\mathbf{p}_1, \mathbf{p}_2$ are two linked points on the tetrahedral model, d is the rest length of the constraint between these two points.

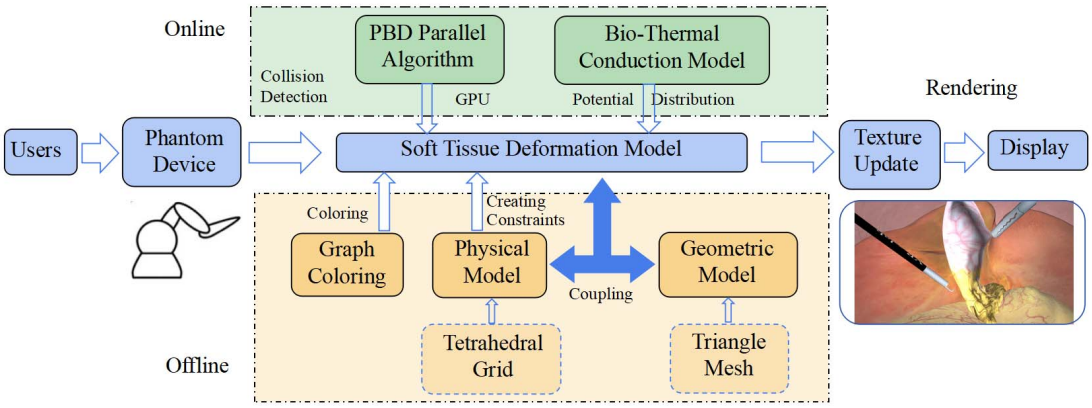

Figure 2: Software architecture of simulation system.

Volume conservation constraints: It can be expressed as:

$$C_{volume}(\mathbf{p}_1,\mathbf{p}_2,\mathbf{p}_3,\mathbf{p}_4) = \frac{1}{6}((\mathbf{p}_2-\mathbf{p}_1)\times(\mathbf{p}_3-\mathbf{p}_1))\cdot(\mathbf{p}_4-\mathbf{p}_1)-V_0, \tag{2}$$

where $\mathbf{p}_1,\mathbf{p}_2,\mathbf{p}_3,\mathbf{p}_4$ are the four vertices of a tetrahedron in the model, V_0 is the rest volume of the tetrahedron before deformation.

In cholecystectomy, the cystic duct/artery are buried in the fat of the Calot triangle region. These tubular tissues usually do not have a large deformation. Thus, we simplify the physical model of tubular tissue, which only contains distance constraints. Instead, the gallbladder is the most important organ in LC. Here we generate multiple constraints for it, which contains distance constraints, volume constraints, attachment constraints, and so on. Solved by the Gauss-Seidel iteration, the final position of each vertex can be updated as follows:

$$\Delta\mathbf{x} = -\lambda_i\omega_i\nabla_{\mathbf{x}}C_i(\mathbf{x}), \tag{3}$$

where λ_i is the Lagrange multiplier, ω_i is the inverse mass of the particle i, and $\nabla_{\mathbf{x}}C_i(\mathbf{x})$ represents the gradient of constraint $C_i(\mathbf{x})$ with respect to $\mathbf{x}$.

3.1.2 Parallelization Strategy of PBD Algorithm

In parallel PBD algorithm, if we directly perform GPU parallel acceleration on the soft tissue deformation solution, parallel computing will cause multi-threaded write conflicts on the constraints with conjunct vertices. Therefore, this paper uses a graph coloring method to color the constraints. In coloring distance constraints, we first treat each distance constraint of tetrahedra as a node (blue point in Fig. 3), then abstract the whole physical system into an undirected graph. In the end, the shared vertex of the constraints is regarded as the undirected edge between two nodes. The distance constraint coloring process is illustrated in Fig. 3. For volume constraints, each tetrahedron is abstracted into a node in an undirected graph. The shared vertex affected by different tetrahedra is treated as an edge between two points in an undirected graph. After graph coloring, any two constraints with the same color but without shared vertices, can be solved in parallel. Through the CUDA parallel library provided by NVIDIA, we first transfer the position, constraints, and colors of vertices from CPU to GPU, then solve the same colored constraints concurrently on the GPU and different colored constraints with the Gauss-Seidel manner. Finally, the data are transferred back to the CPU memory. For different types of constraints, such as distance constraints and volume constraints, coloring initialization and solving processes are performed in sequence. This algorithm combines the advantages of Gauss-Seidel solver for fast iterative convergence and full utilization of GPU parallel acceleration. The parallel PBD on graph coloring can be described as Algorithm 1.

Algorithm 1 Parallel PBD Deformation based on Graph Coloring

Input: At time t, the inputs are the vertex position $\mathbf{x}_i^t$, velocity $\mathbf{v}_i^t$, reciprocal of quality $w_i = 1/m_i$, an external force vector $\mathbf{f}$, time step Δt, and constraints set C of the tetrahedral model.
Output: At time t, updated position $\mathbf{x}_i^{t+1}$, and velocity $\mathbf{v}_i^{t+1}$.

```
i ← 0
Graph coloring the tetrahedral model. Constraints set C = (C_1, C_2, ..., C_k) are divided into several classes, in which each constraint set has its own color c = (c[C_i], i = 1, ·, N), ∀c[C_i] ∈ c. For ∀(C_j, C_m) ∈ C_i, C_j and C_m no sharing point.
loop
  for all Vertices i do
    v_i ← v_i + Δt w_i f_ext(x_i)
  end for
  dampVelocities (v_1, ..., v_n)
  for all Vertices i do
    x_i ← x_i + Δt v_i
  end for
  while solverIterations < MaxIters do
    for all Constraint C_i ∈ C do
      for all Constraint C_ij ∈ C_i do
        projectConstraints(x_i) in parallel on GPU
      end for
    end for
  end while
  for all Vertices i do
    v_i^{t+1} ← (x_i − x_i^t)/Δt
    x_i ← x_i
  end for
end loop
```

For graph coloring (Line 2 in Algorithm 1), we implement coloring partition based on the random dyeing disc graph coloring algorithm [6], and C is the set of constrained abstractions in the graph. The coloring visualization of gallbladder model is illustrated in Fig. 8.

3.2 The Simulation of Electrocautery

The cystic duct/artery are wrapped with the fat. If the gallbladder needs to be removed, the cystic duct/artery are exposed by burning the fat tissue with a L-hook in LC. This process involves electro-thermal conversion, heat conduction, and diffusion. Meanwhile,

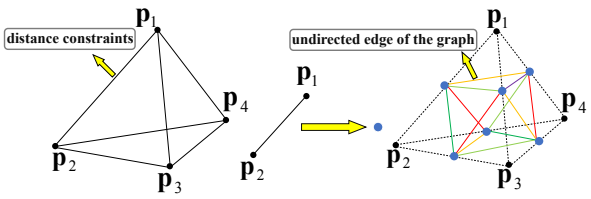

Figure 3: The graph coloring of distance constraints. (a) Each edge in the tetrahedron is a distance constraint, which can be treated as node (blue point) in graph; (b) Abstracting the constraints with a shared vertex into two nodes, which are connected by an undirected edge. Two connected undirected edges denote these constraints having a shared vertex, hence they should be assigned with different color.

for realistic visual effects, smoke and bleeding are also taken into account. Here we focus on how to convert the heat into the potential distribution on the surface of soft tissue. We intend to update the temperature distribution of models based on the bio-heat transfer equation proposed by [4]. The surface bio-heat transfer equation can be expressed as:

$$\rho c \frac{\partial T}{\partial t} = k\nabla^2 T + \omega_b c_b (T - T_\alpha) + q_s + q_{hook}, \tag{4}$$

where ρ is the density of the soft tissue, c represents the heat capacity of the soft tissue, ∇^2 is Laplacian operator. k, ω_b, and c_b represent the thermal conductivity of the soft tissue, the effective blood perfusion flow, and the blood heat capacity respectively. T_α represents the ambient temperature of the blood, q_s represents the fever rate of the organ itself and q_{hook} represents the heat input of the electrocoagulation knife. Since human metabolism and blood flow produce little heat, ω_b, c_b, and q_s can be ignored. Then it can be simplified as:

$$\rho c \frac{\partial T}{\partial t} = k\nabla^2 T + q_{hook}, \tag{5}$$

The second-order differential equation is solved according to the Newmark-beta [30] method which is commonly used in finite element analysis. From this equation, the temperature distribution near the heat source can be calculated. Then, by solving the Laplace equation below [1], the electric field near the contact point between the heat source and the soft tissue is obtained:

$$\nabla \cdot (\sigma \nabla V) = 0, \tag{6}$$

where V represents the potential distribution function and σ represents the electrical conductivity of the soft tissue. Thus, the amount of heat can be obtained by calculating electric field strength with the known current intensity. Fig. 4 shows the temperature distribution when the L-hook touches the surface of gallbladder.

The surface temperature of the soft tissue is stored in the memory as the form of a texture map. During the burning process, we only need to update the local texture map of the touch point. By calculating the projection point $\mathbf{p}'$ of the model that is closest to the haptic device and finding the triangle $Tri(\mathbf{p}_1, \mathbf{p}_2, \mathbf{p}_3)$, where $\mathbf{p}'$ is located, we can obtain the barycentric coordinates $\mathbf{p}$ of the triangle Tri, i.e., $\mathbf{p} = \lambda_1 \mathbf{p}_1 + \lambda_2 \mathbf{p}_2 + \lambda_3 \mathbf{p}_3$. The texture coordinates of the contact point are $\mu = \lambda_1 \mu_1 + \lambda_2 \mu_2 + \lambda_3 \mu_3$, where μ is the texture coordinate of the vertex $\mathbf{p}$. Then the corresponding local temperature distribution texture map can be obtained according to the texture coordinates. The local potential distribution is updated according to the Laplace equation and the thermal surface loss marginal condition. Finally, the temperature distribution is solved and updated according to the heat conduction differential equation.

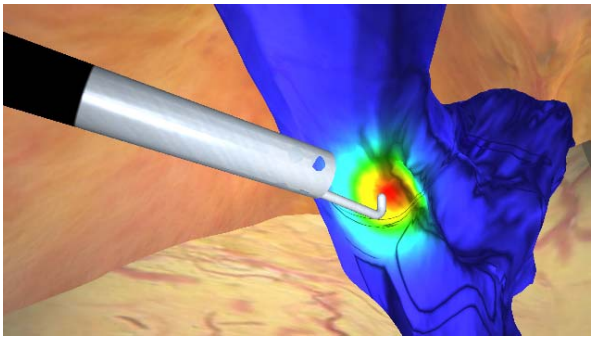

Figure 4: Temperature distribution of bio-thermal conduction electrocautery model on the surface of soft tissue.

In our simulation system, the tetrahedron is coupled with triangle mesh by barycentric coordinates. We can scale the volume to deform the surface mesh to achieve the visual effect of fat tissue burning. Based on the potential distribution on the model, we set a threshold T_v to indicate whether the point on the model is at the boiling point. Generally, there are three states: normal temperature state, heated state, and the burning state. When the vertices in the tetrahedron are not heated, the tetrahedron is at normal temperature. Once one vertex of the tetrahedron reaches the boiling point, the tetrahedron reaches the heated state, but the volume does not change. When two or more vertices of the tetrahedron reach the boiling point, the tetrahedron is at a burning state and the volume would shrink. And the rest length of the constraint will be reduced between the two boiling vertices. When all four vertices of the tetrahedron reach the boiling point state, this tetrahedron is deleted. The whole process can be illustrated in Fig. 5. It can be described as Algorithm 2.

Algorithm 2 The Simulation of Fat Tissue Electrocautery

Input: Fat vaporization temperature T_v, the potential distribution V of the model, initial physical model Tet, the device contact point location $\mathbf{x}$.
Output: The physical model after volume change Tet'.

```
Calculate the distance d between the contact point between device and the model from collision detection.
if d == 0 then
    Update the potential distribution V' of the contact point x.
    for all tetrahedra i do
        num = judegeNumberBoilingPoint(Tet_i, T_v)
        if num == 1 then
            Tet_i reaches the heated state, the volume does not change.
        else if 1 < num < 4 then
            Tet_i reaches burning state, the volume would shrink.
        else if num == 4 then
            Tet_i reaches vaporization state, the tetrahedron is deleted.
        end if
        Tet_i' = updateTetModel(Tet_i)
    end for
end if
```

3.3 The Simulation of Liver and Gallbladder Separation

The separation of the gallbladder from the liver is also an important task in cholecystectomy. In simulation system, the liver and gallbladder are two separated physical models. But in real surgery, there are membrane tissues between the gallbladder and the liver to connect them. Here we propose a hybrid connection model, which employs a

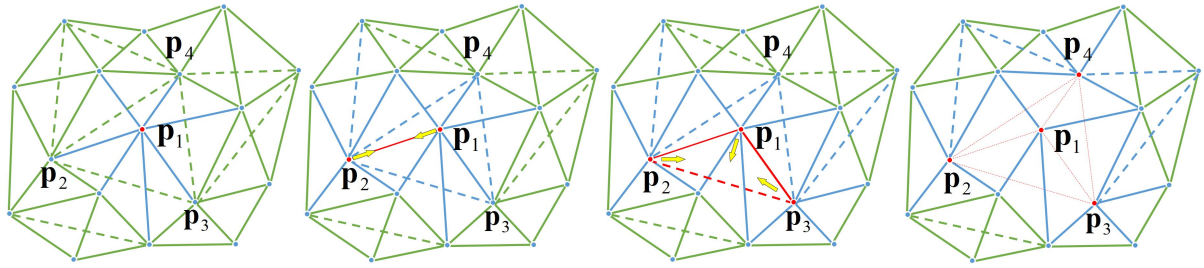

Figure 5: The simulation of fat tissue burning process. (a) The red point p1 indicates that its potential has reached the threshold T (boiling point). Consequently, the tetrahedron is in the heated state (blue edges), but the length is unchanged; (b) p1 and p2 reach the boiling point, then the tetrahedron begins to burn. The red edge indicates that it is burning and the volume of the tetrahedron begins to decrease; (c) p1, p2, and p3 reach the boiling point; d) Once the four vertices of the tetrahedron are at the boiling point state, the tetrahedron will be deleted.

double-layered grid structure. The outer layer is the rendering layer, and the inner layer is the surface mesh of the liver model. Since the membrane tissues between the gallbladder and the liver will be scorched during the separation process, the rendering layer is used to simulate the visual effects, and the inner layer is used to simulate the physical operation. To construct this hybrid connection model, we choose the closed vertices on both the inner surface of gallbladder and liver, and create distance constraints to link these vertices. Then we add these constraints into the solver and solve it iteratively to achieve the connection between the liver and the gallbladder.

In the simulation of separation, we delete the current constraint when the heat source is closed to the junction region between the gallbladder and the liver. Meanwhile, we apply the dynamic texture in OpenGL to implement the rendering of membrane. As mentioned in the previous section, we first obtain the local temperature map coordinates of the gallbladder and the liver through texture coordinates, and then use the bio-thermal conduction model to calculate the temperature and update the texture accordingly. To better simulate the physiological characteristics of organs during electrocautery, we interpolate the colors to demonstrate the change from flesh to browning when the membrane is burned. When starting to burn, it is initialized to white $C_1 = (1.0, 1.0, 1.0, 0.0)$, and after burning, it becomes $C_2 = (1.0, 0.92, 0.80, 0.7)$. Finally, the color of membrane tissue is set as $C_3 = (1.0, 0.82, 0.70, 0.2)$. The interpolation function for updating the texture is:

$$C_{mix} = (1-k)C + kC_i, i = 1, 2, 3, \tag{7}$$

where C is the initial color, k is the color change factor, and $k = min((T - T_0)/(T_v - T_0), 1.0)$. T is the current temperature, T_0 is the ambient temperature, and T_v is the threshold of the burning temperature. We set $k_{change} = 0.8$ and $k_{vaporization} = 0.99$. The value i is:

$$i = \begin{cases} 1, & k \le k_{change} \\ 2, & k_{change} < k \le k_{vaporization} \\ 3, & otherwise \end{cases}.$$

3.4 Haptic Rendering

We use the OpenHaptics library to develop the force feedback. The library provides the function access. Besides the main program, it creates two background programs for tactile calculation and rendering. A thread (named service thread) mainly collects the spatial position coordinates and rotation angles of the force feedback device, and transmits the feedback force to the haptic device continuously. The refresh frequency of this thread is 1000Hz. Fig. 6 illustrates a section of force curve in haptic rendering. Another thread is called collision thread, which mainly deals with the collision detection and response. The refresh frequency of this thread is 100Hz. We use the data provided by these threads to calculate the force. It contains a vector of outward normal for the mesh surface and a magnitude, which is proportional to the depth of instrument sunk into the tissue. The parameter coefficient can be set based on biological experiments.

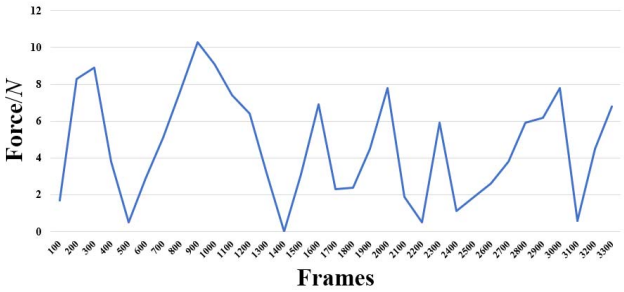

Figure 6: Force curve in haptic rendering.

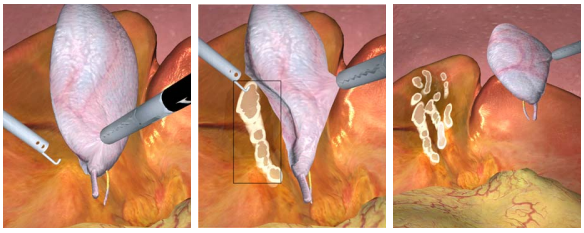

Figure 7: The simulation results of the liver-gallbladder separation. (a) Before separation; (b) During separation (burning marks in black rectangle); (c) After seperation.

4 Experiments and Validation

4.1 Experimental Settings and Implementation Details

The computer used for simulation is a Lenovo desktop (NVIDIA GeForce GTX 980Ti, Intel Core i7-4770 3.4GHz, 8GB RAM). We modified two surgical handles (L-hook and grasper) which are connected with two phantom devices. The foot pedal is used to control

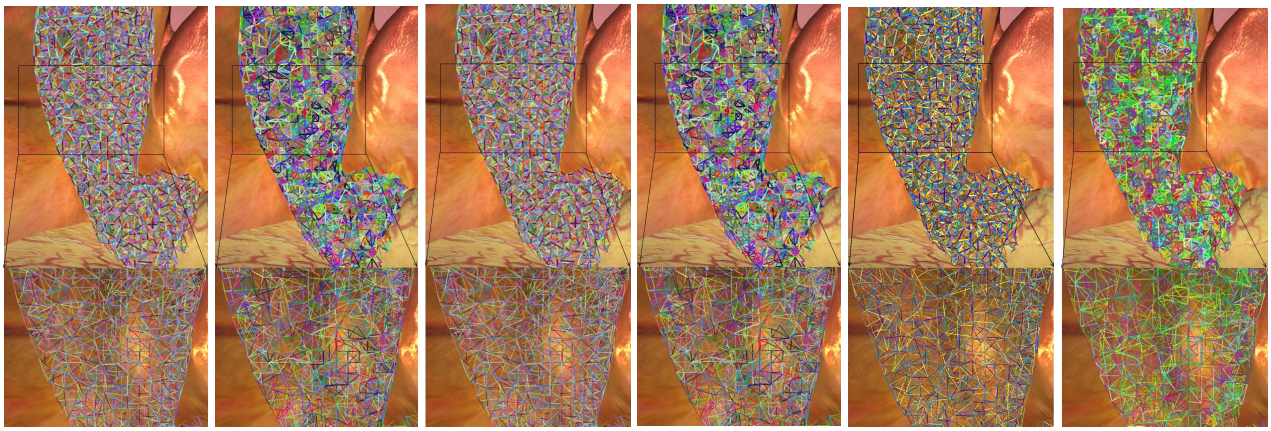

Figure 8: Visualization results of coloring the gallbladder model based on the random dyeing disc algorithm, the maximum independent set coloring algorithm and the greedy heuristic coloring algorithm. (a)-(c) are the results for the distance constraint, (d)-(f) are the results for the volume constraint.

the electric burning of L-hook when trampled. The algorithms proposed in this paper are not surgery and patient specific. We can change the anatomical 3D models for other types of procedure training using our simulator. We design three experiments to test the simulation results and analyze the computational costs of algorithms. In the first experiment, the computational cost of our deformation method of graph coloring are tested. Appendix A documents several parameters setting in the system after feedback from surgeons. We implement three graph coloring algorithms (maximum independent set staining algorithm [14], greedy heuristic shading algorithm [27] and random dyeing disc algorithm). Fig. 8 shows the results of graph coloring for the distance constraints and volume constraints. Fig. 9 is the simulation results in LC at 0ms, 25ms, 50ms, and 100ms after the gallbladder is dragged. We can find that the gallbladder converges to the initial shape shortly after large deformation. In the second experiment, we test our simulation method of electrocautery. Fig. 10 illustrates the process of burning fat tissue, including the visual effect of smoke generation and bleeding. Fig. 11 shows the detail of topology change of the gallbladder mesh when fat is burned. The third experiment demonstrates the simulation results of the liver-gallbladder separation. In Fig. 7, we can clearly find the burning traces left by the L-hook after electrocautery. Finally, the pie chart in Fig. 12 shows the computational costs of each task during offline and online phases respectively. The most time-consuming task in the offline phase is the tetrahedron initialization, which takes about 2886ms. The most time-consuming task in online phase is the parallel PBD deformation, which takes about 16.5ms.

4.2 Comparisons

We also compare algorithms in our system with other approaches. First, we implemented the maximum independent set coloring and the greedy heuristic coloring for comparison of the dyeing effects used in our simulator (Tab. 1). We find that the algorithm based on the largest independent set uses the biggest number of colors, and the coloring algorithm based on the random dyeing disc performs the best. Therefore, we choose the coloring algorithm based on random dyeing disc to accelerate our PBD model. Tab. 2 illustrates the acceleration effects of the parallel PBD model compared with the ordinary PBD model. We can find that this algorithm has a great advantage for real-time simulation. However, the improvement of performance using our dying algorithm is not as high as we expected. The main reason is that different groups of constraints are solved

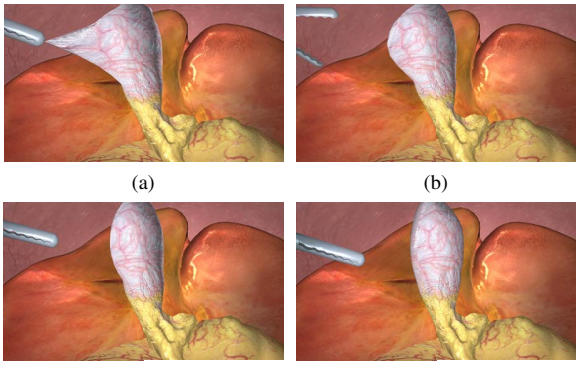

Figure 9: The deformation of gallbladder after dragging. (a) 0ms, (b) 25ms, (c) 50ms, (d) 100ms.

serially. The second reason is that the number of constraints for each color is not in good balance. Tab. 1 shows that 10% color classification only contains 0.2% constraints, hence it is very unbalanced and increasing the calculation cost.

Next, we compare the data size and visual performance with the work of Kim et al. [11]. Our computation costs are significantly lower than [11] (Tab. 3), since the advantage of our method is obvious when simulating complex models. Besides, we introduce a bio-thermal conduction model to the fat tissue burning. It further increases the physical authenticity of the simulation. Finally, we use dynamic texture techniques to render the process of stripping the gallbladder from the liver. During electrocautery with the L-hook, the liver surface will leave burning traces, which enhance the visual realism (Fig. 13).

4.3 Validation and Discussion

We invited 32 surgeons from Beijing Aerospace General Hospital to test and evaluate our simulator. All participants were right-handed. After evaluation, they will complete a survey to give us feedback. We design a questionnaire which contains 10 questions: (1) Realism of the anatomy; (2) The authenticity of the simulator scene; (3)

Table 1: Comparison of three graph coloring algorithms.

Color algorithm	Color size	Top 10% colors	Middle 80% colors	Last 10% colors	Time cost per step (ms)
Greedy	32	0.354	0.645	0.001	12.65-12.98
Maximum independence	36	0.195	0.801	0.004	14.06-14.23
Random coloring disk	32	0.320	0.679	0.002	12.20-12.35

Table 2: Comparison of parallel PBD and ordinary PBD simulation results for gallbladder model (0.2ms time step, 30 iterations, Random dyeing disc algorithm).

Vertices	Links	Tets	parallel PBD on GPU		PBD on CPU
			Time cost per step (ms)	Colors	Time cost per step (ms)
3966	21076	13125	14.31-14.42	40	16.38-17.41
6823	32256	22650	12.20-12.35	32	28.51-29.10
10608	56503	35056	14.49-14.57	36	45.79-47.36
12481	66366	41144	16.36-16.47	40	54.81-55.65
20869	110459	68338	21.65-22.16	39	111.51-116.38

Table 3: Comparison of data size and computational efficiency with respect to the work of Kim et al. [11].

Methods	No. of tetrahedra (Liver)	No. of tetrahedra (Galllbladder)	FPS
Kim et al.	518	108	29.3
	5024	470	12.4
	10615	817	7.3
Ours	5176	519	84.75
	12876	883	82.64
	19729	22611	57.44

Table 4: Statistics of the questionnaire.

Question	Mean	SD	Question	Mean	SD
1	7.5	0.26	6	7.8	0.54
2	8.1	0.62	7	7.6	0.46
3	7.0	0.34	8	6.5	0.44
4	6.9	1.19	9	6.5	0.47
5	7.7	0.79	10	8.0	0.54

Authenticity of surgical instruments; (4) The authenticity of the view coordinate system; (5) Authenticity of soft tissue deformation; (6) The authenticity of the fat tissue burning; (7) Authenticity of hepatobiliary separation process; (8) Quality and authenticity of force feedback; (9) Practice of the hand-eye coordination; and (10) The utility of the system compared to traditional training methods. The scores for these questions range from 0-10, where 0 represents the worst and 10 represents the most satisfactory. Fig. 14 is the picture when surgeons manipulate our simulator. Tab. 4 documents the average scores for the 10 questions. It also indicates which aspects need to be improved. In Tab. 4, the overall utility of the simulator, the soft tissue deformation, the authenticity of the fat tissue burning, and the authenticity of the hepatobiliary separation have reached a good level (7.5 or higher on average). The realism of the anatomy is also quite good, indicating the authenticity of our simulator. The lowest score is "Quality and authenticity of force feedback", and we need to make more efforts to improve in the near future.

We also record the completion time of training tasks for each trainee to evaluate their performance. In our system, the surgeons force feedback (Fig. 6) and time in manipulation can be recorded and displayed. After collecting all statistical data, the average completion time for LC procedure training is 25 minutes and force ranges from 0-12N. This roughly corresponds to the time and force range of a practical LC procedure in clinic. Finally, we interviewed all the participants and 91 percent agreed that the simulator played a positive role in laparoscopic surgery training. 82 percent think that we should apply the laparoscopic surgery simulator to the daily medical education. Compared with the real surgery, they believed that there is still room for improvement in force feedback. In visual performance, the boundary between the gallbladder and the liver is too obvious. In the real operation, the boundary between these two organs is close and fuzzy.

5 Conclusion and Future Works

In this paper, we have developed a VR-based laparoscopic cholecystectomy simulation system. First, we used the GPU to accelerate the deformation model and obtain a better computation performance by applying the random dyeing disc algorithm. Meanwhile, we introduced a physical model based on bio-heat conduction in the fat tissue electrocautery. A more realistic burning path could be achieved based on the heat transfer temperature strategy. Then the topology and the surface texture were updated by modifying the tetrahedral constraints. Finally, we separated the liver and gallbladder with a hybrid multi-model connection model, which enhances the visual effect by adding realistic rendering such as smoke and bleeding.

Nevertheless, there are certain limitations in our simulation. Due to the intrinsic shortcoming of PBD method, the stiffness of the organ model is sensitive to the number of iterations and the step size. But it could be eliminated with extended position-based dynamics (XPBD) [16], which can be employed in our simulator in the near

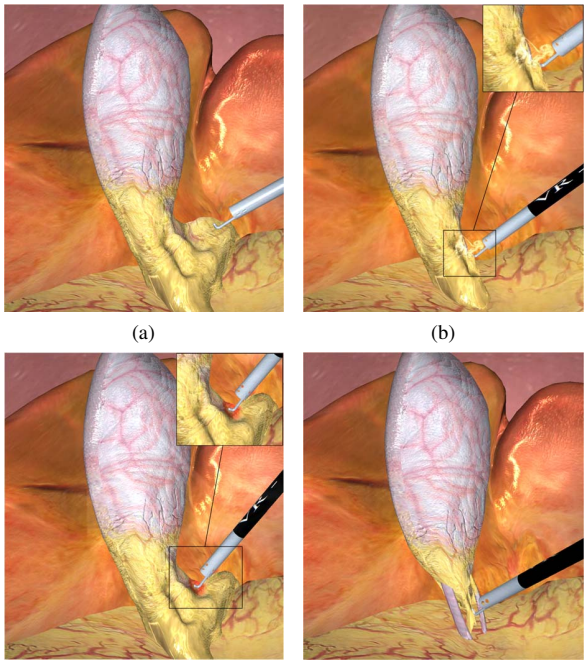

(a) (b) (c) (d)

Figure 10: The simulation results of electrocautery in LC, including smoke and bleeding.

future. At present, Phantom Omni only supports single point force feedback, a trainee can merely grab a point or a few points in local area when grabbing the soft tissue. To achieve more realistic results, we need to improve the haptic device to achieve multi-point contact. Moreover, we can develop the evaluation system, which can afford a reminder when operation error happens and deliver the score report after the training is completed.

ACKNOWLEDGMENTS

This research is supported in part by National Key R&D Program of China (No. 2018YFC0115102), National Natural Science Foundation of China (NO. 61872020, 61532002, 61672149), Beijing Natural Science Foundation Haidian Primitive Innovation Joint Fund (L182016), Beijing Advanced Innovation Center for Biomedical Engineering (ZF138G1714), and NSF IIS-1715985 and NSF IIS-1812606 of USA. We also thank the Faculty of Media and Communication, Bournemouth University (UK) with its support of Global Visiting Fellowship for Dr. Junjun Pan.

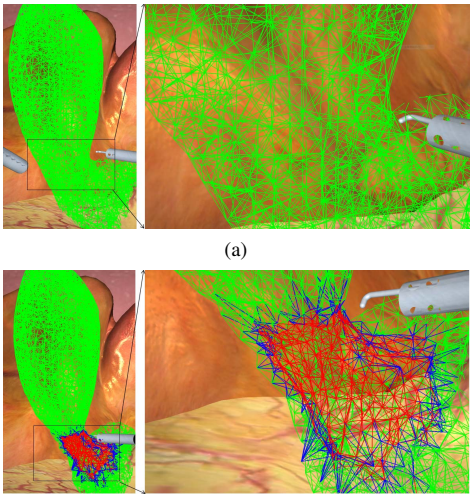

(a) (b)

Figure 11: The topology change of fat tissue mesh before (a) and after (b) electrocautery.

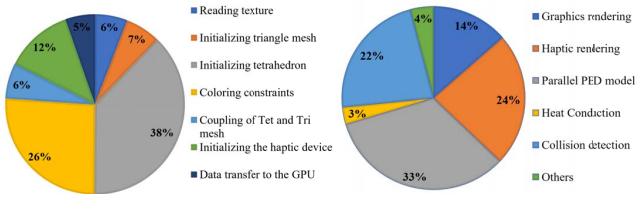

(a) (b)

Figure 12: The percentage of computational cost for each task. (a) Offline phase; (b) Online phase.

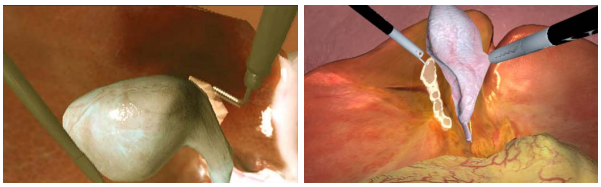

(a) (b)

Figure 13: Comparison of simulation visual performance with the work of Kim et al [11]. (a) The screenshot in [11]; (b) The screenshot of our simulator.

Figure 14: Surgeons are evaluating our system.

REFERENCES

[1] E. J. Berjano. Theoretical modeling for radiofrequency ablation: state-of-the-art and challenges for the future. *Biomedical engineering online*, 5(1):24, 2006.

[2] I. Berndt, R. Torchelsen, and A. Maciel. Efficient surgical cutting with position-based dynamics. *IEEE computer graphics and applications*, 37(3):24–31, 2017.

[3] S. L. Delp, P. Loan, C. Basdogan, and J. M. Rosen. Surgical simulation: An emerging technology for training in emergency medicine. *Presence: Teleoperators & Virtual Environments*, 6(2):147–159, 1997.

[4] R. E. Dodde, S. F. Miller, J. D. Geiger, and A. J. Shih. Thermal-electric finite element analysis and experimental validation of bipolar electro-surgical cautery. *Journal of manufacturing science and engineering*, 130(2):021015, 2008.

[5] M. Fratarcangeli. Position-based facial animation synthesis. *Computer Animation and Virtual Worlds*, 23(3-4):457–466, 2012.

[6] M. Fratarcangeli, V. Tibaldo, and F. Pellacini. Vivace: a practical gauss-seidel method for stable soft body dynamics. *ACM Transactions on Graphics (TOG)*, 35(6):214, 2016.

[7] D. A. Grable and A. Panconesi. Fast distributed algorithms for brooks–vizing colorings. *Journal of Algorithms*, 37(1):85–120, 2000.

[8] C. Healthcare. Cae lapvr. Website, 2020. `https://caehealthcare.com/surgical-simulation/lapvr/`.

[9] Z. M. G. Inc. Human anatomy. Website, 2020. `http://www.3dscience.com/3D_Models/index.php`.

[10] M. T. Jones and P. E. Plassmann. A parallel graph coloring heuristic. *SIAM Journal on Scientific Computing*, 14(3):654–669, 1993.

[11] Y. Kim, L. Kim, D. Lee, S. Shin, H. Cho, F. Roy, and S. Park. Deformable mesh simulation for virtual laparoscopic cholecystectomy training. *The Visual Computer*, 31(4):485–495, 2015.

[12] Y. Kim, S. Lee, F. Roy, D. Lee, L. Kim, and S. Park. Carving mesh with deformation for soft tissue removal simulation. In *Workshop on Mesh Processing in Medical Image Analysis*, pp. 70–79. Springer, 2012.

[13] Z. Lu, V. S. Arikatla, Z. Han, B. F. Allen, and S. De. A physics-based algorithm for real-time simulation of electrosurgery procedures in minimally invasive surgery. *The International Journal of Medical Robotics and Computer Assisted Surgery*, 10(4):495–504, 2014.

[14] M. Luby. A simple parallel algorithm for the maximal independent set problem. *SIAM journal on computing*, 15(4):1036–1053, 1986.

[15] D. Luo, Y. Zhang, and R. Zhao. Study on deformation technology of virtual surgery simulator based on liver puncture. In *2018 3rd International Conference on Robotics and Automation Engineering (ICRAE)*, pp. 176–179. IEEE, 2018.

[16] M. Macklin, M. Müller, and N. Chentanez. Xpbd: position-based simulation of compliant constrained dynamics. In *Proceedings of the 9th International Conference on Motion in Games*, pp. 49–54. ACM, 2016.

[17] S. Misra, K. Ramesh, and A. M. Okamura. Modeling of tool-tissue interactions for computer-based surgical simulation: a literature review. *Presence: Teleoperators and Virtual Environments*, 17(5):463–491, 2008.

[18] M. Müller, B. Heidelberger, M. Hennix, and J. Ratcliff. Position based dynamics. *Journal of Visual Communication and Image Representation*, 18(2):109–118, 2007.

[19] M. Müller, J. Stam, D. James, and N. Thürey. Real time physics: class notes. In *ACM SIGGRAPH 2008 classes*, p. 88. ACM, 2008.

[20] J. Pan, J. Bai, X. Zhao, A. Hao, and H. Qin. Real-time haptic manipulation and cutting of hybrid soft tissue models by extended position-based dynamics. *Computer Animation and Virtual Worlds*, 26(3-4):321–335, 2015.

[21] RESEARCH and MARKETS. Global laparoscopy and endoscopy devices market: Focus on surgical procedures (cholecystectomy and hysterectomy) and product types (arthroscopes, neuroendoscopes, cystoscope, and bronchoscopes) - analysis and forecast, 2018-2025. Website, 2020. `https://www.researchandmarkets.com/research/626pqp/global?w=12`.

[22] G. Sankaranarayanan, R. R. Resapu, D. B. Jones, S. Schwaitzberg, and S. De. Common uses and cited complications of energy in surgery. *Surgical endoscopy*, 27(9):3056–3072, 2013.

[23] S. Science. Lapsim surgical science simulator. Website, 2020. `https://surgicalscience.com/systems/lapsim/`.

[24] D. Systems. Lap mentor (formerly simbionix lap mentor). Website, 2020. `https://simbionix.com/simulators/lap-mentor/lap-mentor-vr-or/`.

[25] D. Systems. Phantom omni. Website, 2020. `https://www.3dsystems.com/haptics-devices/touch`.

[26] A. Talvas, M. Marchal, C. Duriez, and M. A. Otaduy. Aggregate constraints for virtual manipulation with soft fingers. *IEEE transactions on visualization and computer graphics*, 21(4):452–461, 2015.

[27] M. K. Tas, K. Kaya, and E. Saule. Greed is good: Parallel algorithms for bipartite-graph partial coloring on multicore architectures. In *2017 46th International Conference on Parallel Processing (ICPP)*, 2017.

[28] R. Wang, J. Yao, L. Wang, X. Liu, H. Wang, and L. Zheng. A surgical training system for four medical punctures based on virtual reality and haptic feedback. In *2017 IEEE symposium on 3D user interfaces (3DUI)*, pp. 215–216. IEEE, 2017.

[29] L. Xiong, G. Jiang, Y. Guo, and H. Liu. A three-dimensional fiber bragg grating force sensor for robot. *IEEE Sensors Journal*, 18(9):3632–3639, 2018.

[30] O. Zienkiewicz and T. Shiomi. Dynamic behaviour of saturated porous media; the generalized biot formulation and its numerical solution. *International journal for numerical and analytical methods in geomechanics*, 8(1):71–96, 1984.

Appendices

A RELATED PARAMETERS SETTING IN OUR SIMULATION SYSTEM

Parameters	Value
Stiffness of stretch	0.4
Length of time step (s)	0.2
Density (kg/m^3)	3
Liver model vertices	2626
Specific heat ($J/kg \cdot K$)	0.3
Number of terahedra(liver)	19729
Stiffness of volume	908
Gallbladder model vertices	6823
Electrical conductivity (S/m)	0.9
Number of iterations (gallbladder)	30
Thermal conductivity (N/m^2)	0.512
Number of tetrahedra (gallbladder)	35056